

EFFECTIVE DYNAMICS FOR N -SOLITONS OF THE GROSS-PITAEVSKII EQUATION

TREVOR POTTER

ABSTRACT. We consider several solitons moving in a slowly varying external field. We show that the effective dynamics obtained by restricting the full Hamiltonian to the finite dimensional manifold of N -solitons (constructed when no external field is present) provides a remarkably good approximation to the actual soliton dynamics. That is quantified as an error of size h^2 where h is the parameter describing the slowly varying nature of the potential. This also indicates that previous mathematical results of Holmer-Zworski [8] for one soliton are optimal. For potentials with unstable equilibria the Ehrenrest time, $\log(1/h)/h$, appears to be the natural limiting time for these effective dynamics. We also show that the results of Holmer-Perelman-Zworski [7] for two mKdV solitons apply numerically to a larger number of interacting solitons. We illustrate the results by applying the method with the external potentials used in Bose-Einstein soliton train experiments of Strecker *et al* [14].

1. INTRODUCTION

In many situations a wave moving in a slowly varying field, that is, a field described by a potential whose derivatives are much smaller than the oscillations/width of the wave, can be described using classical dynamics. This is the basis of the semiclassical/short wave approximation, perhaps best known in the case of the linear Schrödinger equation,

$$(1.1) \quad ih\partial_t u = -\frac{1}{2}h^2\partial_x^2 u + V(x)u,$$

where V is an infinitely differentiable potential. A typical result concerns a propagation of a coherent state

$$u(x, 0) = \exp\left(\frac{i}{h}\left((x - x_0)\xi_0 + i(x - x_0)^2/2\right)\right),$$

maximally concentrated near the point (x_0, ξ_0) in the position-momentum space. In that case,

$$(1.2) \quad u(x, t) = a_0(x, t) \exp\left(\frac{i}{h}\varphi(x, t)\right) + \mathcal{O}(h^{\frac{1}{2}}), \quad 0 < t < T(h),$$

where $\text{Im } \partial_x^2 \varphi > 0$, $\text{Im } \varphi \geq 0$, and

$$\text{Im } \varphi(x, t) = 0 \Rightarrow x = x(t), \quad \partial_x \varphi(x, t) = \xi(t),$$

where $(x(t), \xi(t))$ satisfy Newton's equations:

$$(1.3) \quad x'(t) = \xi(t), \quad \xi'(t) = -V'(x), \quad x(0) = x_0, \quad \xi(0) = \xi_0.$$

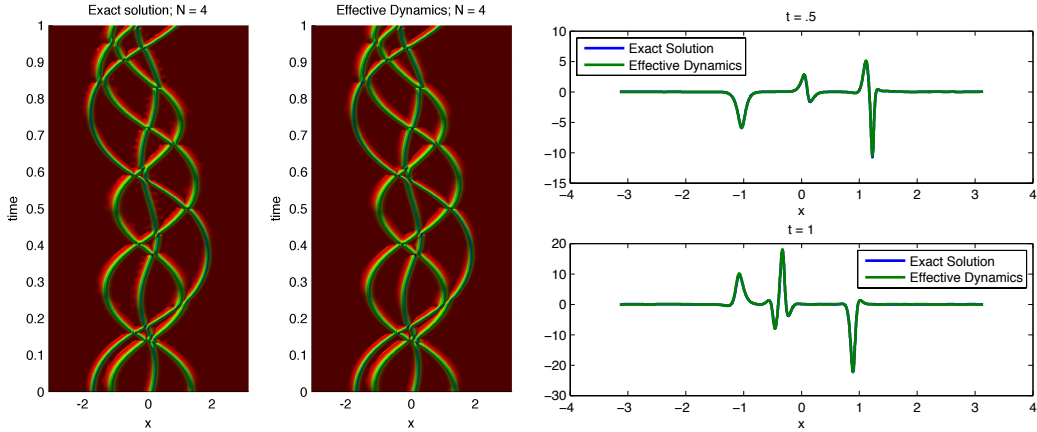


FIGURE 1. A side-by-side comparison of the effective dynamics versus the exact solution of (1.6) for 4 solitons with the potential $W(x) = -100e^{\cos x}$. The plot on the left shows the absolute value of the solutions up to time $t = 1$. The plot on the right shows the real part of the solutions at times $t = 0.5$ and $t = 1$. Compared to the solutions in Figures 4 and 5, much less discrepancy between the two solutions is visible.

The time of the validity of (1.2), $T(h)$, depends on the properties of the flow (1.3), and in general it is limited by the *Ehrenfest time*,

$$(1.4) \quad T(h) \sim \log \left(\frac{1}{h} \right),$$

see [1] for a recent discussion on the case of one dimension.

The approximation (1.2) means that the solution is concentrated for logarithmically long times on classical trajectories. The phase φ and the amplitude a_0 can be described very precisely and a_0 can be refined to give an asymptotic expansion – see [6] for an early mathematical treatment and [13] for more recent developments and references.

In this paper we consider the Gross-Pitaevski equation, which is the cubic non-linear Schrödinger equation with a potential:

$$(1.5) \quad ih\partial_t u = -\frac{1}{2}h^2\partial_x^2 u - u|u|^2 + V(x)u.$$

It provides a mean field approximation for the evolution of Bose-Einstein condensate in an external field given by the potential $V(x)$ – see the monograph [12] and references given there. Questions about propagation of localized states are also natural in the setting of (1.5) and have been much studied. One direction is described in a recent monograph [2].

In this note we present a numerical study of multiple soliton propagation for (1.5) and show that it can be described very accurately using a natural effective dynamics – see Figure 1. That effective dynamics is based on mathematical results of Holmer-Zworski [8] and Holmer-Perelman-Zworski [7] and we refer to those papers for pointers to earlier mathematical works on that subject.

Following the convention of earlier papers – see Fröhlich et al [4] – we rescale equation (1.5) so that the parameter h is in the potential which is now slowly varying:

$$(1.6) \quad i\partial_t u = -\frac{1}{2}\partial_x^2 u - u|u|^2 + V(x)u, \quad V(x) = W(hx).$$

For $V \equiv 0$ this equation is completely integrable – see for instance [3]. One of the most striking consequences of that is the existence of exact N -soliton solutions:

$$(1.7) \quad \begin{aligned} u(x, t) &= q_N(x, a + tv, v, \theta + \frac{t}{2}(\mu^2 + v^2), \mu), \\ a, v &\in \mathbb{R}^N, \quad \theta \in (\mathbb{R}/2\pi\mathbb{Z})^N, \quad \mu \in \mathbb{R}_+^N, \end{aligned}$$

where the construction of $q_N = q_N(x, a, v, \theta, \mu)$ will be recalled in §2.

When $V \not\equiv 0$ and

$$u(x, 0) = q_N(x, a, v, \theta, \mu),$$

the exact dynamics (1.7) is replaced by

$$(1.8) \quad u(x, t) = q_N(x, a(t), v(t), \theta(t), \mu(t)) + \mathcal{O}(h^2),$$

where the precise meaning of the error, and its optimality, will be described below. The parameters of the multisoliton approximation solve the system of ordinary differential equations:

$$(1.9) \quad \begin{aligned} \dot{v}_j &= -\mu_j^{-1}(\partial_{a_j} V_N + v_j \partial_{\theta_j} V_N), \quad \dot{a}_j = v_j + \mu_j^{-1} \partial_{v_j} V_N, \\ \dot{\mu}_j &= \partial_{\theta_j} V_N, \quad \dot{\theta}_j = v_j^2/2 + \mu_j^2/2 + \mu_j^{-1} v_j \partial_{v_j} V_N - \partial_{\mu_j} V_N, \end{aligned}$$

and where

$$V_N(a, v, \theta, \mu) \stackrel{\text{def}}{=} \frac{1}{2} \int_{\mathbb{R}} V(x) |q_N(x, a, v, \theta, \mu)|^2 dx.$$

Although somewhat complicated looking, the equations (1.9) have a natural interpretation in terms of Hamiltonian systems: they are the Hamilton-Jacobi equations for the full Hamiltonian of (1.6) restricted to the symplectic $4N$ -dimensional manifold of N -solitons – see §3 for details. Of course when $V \equiv 0$ the solutions correspond to the exact solutions of (1.7). The mathematical results of [7], [8] suggest that the approximation (1.8) is valid up to a (rescaled) Ehrenfest time (1.4):

$$(1.8) \text{ holds for } 0 < t < C \log(1/h)/h.$$

In other words, the equations (1.9) give the minimal exact effective dynamics valid up to the Ehrenfest time $\log(1/h)/h$, where h is the parameter controlling the small variation of the potential, see (3.1). In this work, we show that the approximation errors $\mathcal{O}(h^2)$ and the Ehrenfest time bound are sharp. See [11] for a survey of soliton dynamics under integrable systems that have been perturbed.

One motivation for this study is the experimental and theoretical investigation of soliton trains in Bose-Einstein condensates [14]. We show that the effective dynamics described in §3 is in qualitative agreement with the behaviour of the matter-wave soliton trains – see Figure 2.

The paper is organized as follows: in §2 we recall the construction of N -soliton solutions for $V \equiv 0$ and in §3, the Hamiltonian structure of the equation and the derivation of the effective equations of motion. In §4 we compare the effective dynamics to the behaviour

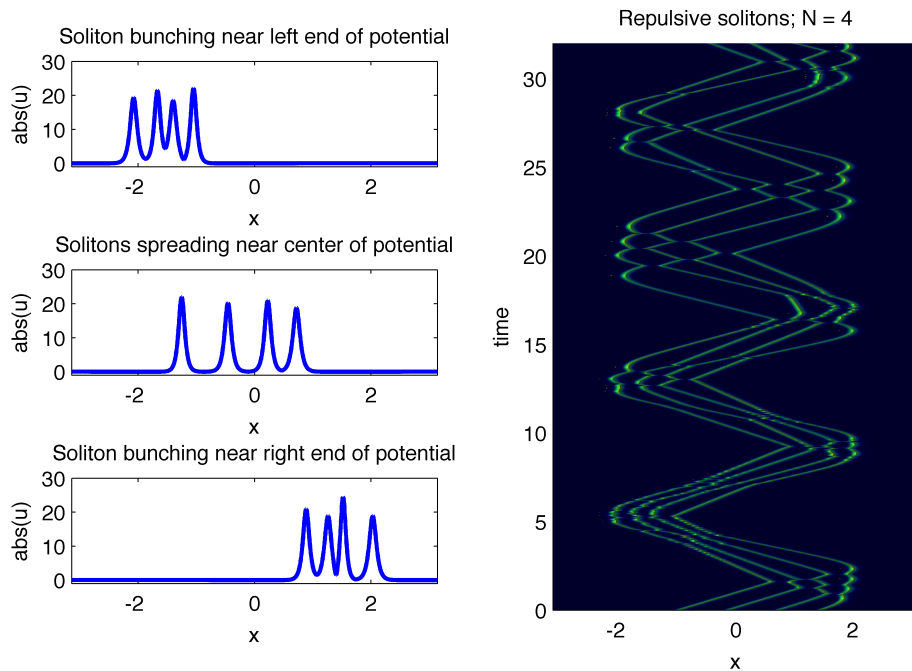


FIGURE 2. Four solitons with alternating phases bunching up and spreading out in the potential $V(x) = (x/2)^6$. The full solution is plotted on the right with a bird's eye view. The figures on the left are snapshots of that solution. Due to their alternating phases, the solitons repel and never pass through each other.

of solutions to (1.6) and draw some quantitative conclusions. Specific potentials similar to those in [14] are then discussed in §5. We investigate effective dynamics for the mKdV equation in §6. Finally, in §7 we describe the numerical methods and compare to other possible approaches.

2. N -SOLITONS FOR CUBIC NLS

When $V \equiv 0$, we recover the nonlinear cubic one dimensional Schrödinger equation, which has N -soliton solutions with explicit formulas that we now recall – see [3] for a detailed presentation of this completely integrable equation.

We will construct functions $q_N(x)$ that depend on $4N$ parameters: positions, velocities, phases, and masses:

$$(2.1) \quad q_N(x) = q_N(x, a, v, \theta, \mu), \quad a, v, \theta \in \mathbb{R}^N, \quad \mu \in (0, \infty)^N.$$

Put

$$(2.2) \quad \lambda_j = v_j + i\mu_j, \quad \gamma_j(x) = e^{i\lambda_j x} e^{i(\theta_j - v_j a_j)} e^{\mu_j a_j},$$

and define matrices

$$M(x) \in \mathbb{R}^{N \times N}, \quad M_1(x) \in \mathbb{R}^{(N+1) \times (N+1)},$$

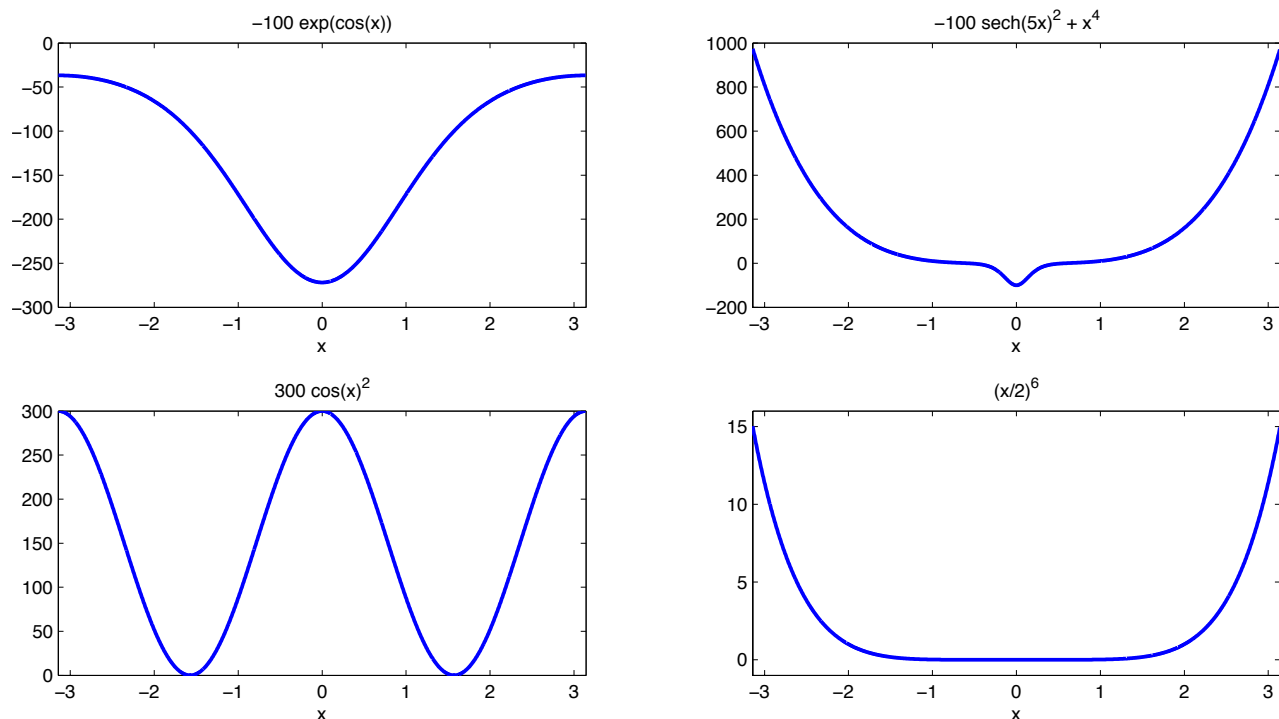


FIGURE 3. A gallery of potentials used for the numerical experiments. Since the solitons in the experiments have width approximately $1/10$, the interesting potentials should have size approximately 100. This is suggested by the rescaling (3.9). The potentials vary on a scale comparable to 1, hence the effective h is approximately $1/10$. The exception is the upper right plot where we intentionally chose a potential which will exhibit some failures of effective dynamics. In the analysis of errors, for instance in Figure 6, only relative sizes of h matter.

by

$$(2.3) \quad M_{jk}(x) = \frac{1 + \gamma_j(x)\bar{\gamma}_k(x)}{\lambda_j - \bar{\lambda}_k}, \quad M_1 = \begin{bmatrix} M(x) & \gamma \\ \vec{1} & 0 \end{bmatrix}$$

where

$$(2.4) \quad \gamma = [\gamma_1, \dots, \gamma_N]^T, \quad \vec{1} = [1, \dots, 1] \in \mathbb{R}^N.$$

Finally,

$$(2.5) \quad q_N(x) \stackrel{\text{def}}{=} \frac{\det M_1(x)}{\det M(x)}.$$

Remarkably, this gives a solution to (1.5) with $V \equiv 0$, the N -soliton solution:

$$(2.6) \quad u(x, t) = q_N(x, a + tv, v, \theta + \frac{t}{2}(\mu^2 + v^2), \mu).$$

As one can see from the formula, some restrictions on the parameters apply, see [3].

3. EFFECTIVE DYNAMICS EQUATIONS

We consider potentials defined on \mathbb{R} that are slowly varying in the sense that

$$(3.1) \quad V(x) = W(hx)$$

where $W(x)$ is C^2 in x , and

$$|\partial_x^k W(x)| \leq C(1 + |x|)^N, \quad k \leq 2.$$

where C and N are independent of h . This means that h is the parameter controlling the slow variation of V .

To obtain an effective dynamics for the evolution we use the Hamiltonian structure of the equation. In the physics literature an approach using Lagrangians is more common – see for instance Goodman-Holmes-Weinstein [5] and Strecker et al [14]. In the mathematics treatments [4],[8],[7] the Hamiltonian approach was found easier to use, which we follow here.

The basic claim is that an approximate evolution of q_N is obtained by restricting the Hamiltonian flow generated by the Gross-Pitaevskii equation to the manifold of N -solitons described in §2. The Hamiltonian associated with the Gross-Pitaevskii equation is

$$(3.2) \quad H_V(u) \stackrel{\text{def}}{=} \frac{1}{4} \int (|\partial_x u|^2 - |u|^4) dx + \frac{1}{2} \int V|u|^2$$

with respect to the symplectic form

$$(3.3) \quad \omega(u, v) = \text{Im} \int u \bar{v}.$$

The manifold of solitons, M_N , is $4N$ -dimensional and equipped with the restricted symplectic form given by the sum of forms for single solitons:

$$(3.4) \quad \omega_M \stackrel{\text{def}}{=} \omega|_M = \sum_{j=1}^N (\mu_j dv_j \wedge da_j + v_j d\mu_j \wedge da_j + d\theta_j \wedge d\mu_j).$$

H_V restricted to M_N is

$$(3.5) \quad H_N \stackrel{\text{def}}{=} H_V|_{M_N}(a, v, \theta, \mu) = \sum_{j=1}^N \left(\frac{\mu_j v_j^2}{2} - \frac{\mu_j^3}{6} \right) + V_N(a, v, \theta, \mu),$$

$$(3.6) \quad \text{where } V_N(a, v, \theta, \mu) \stackrel{\text{def}}{=} \frac{1}{2} \int_{\mathbb{R}} V(x) |q_N(x, a, v, \theta, \mu)|^2 dx.$$

The effective dynamics is given by the flow of the Hamilton vector field of H_N on the manifold M_N . That vector field, Ξ_{H_N} , is defined using the symplectic form (3.4):

$$(3.7) \quad dH_N = \omega_M(\cdot, \Xi_{H_N}).$$

A computation based on this gives the following ordinary differential equation for the parameters a, v, θ and μ , called the effective dynamics:

$$(3.8) \quad \begin{aligned} \dot{v}_j &= -\mu_j^{-1} \partial_{a_j} H_N - \mu_j^{-1} v_j \partial_{\theta_j} H_N = -\mu_j^{-1} (\partial_{a_j} V_N + v_j \partial_{\theta_j} V_N), \\ \dot{a}_j &= \mu_j^{-1} \partial_{v_j} H_N = v_j + \mu_j^{-1} \partial_{v_j} V_N, \\ \dot{\mu}_j &= \partial_{\theta_j} H_N = \partial_{\theta_j} V_N, \\ \dot{\theta}_j &= \mu_j^{-1} v_j \partial_{v_j} H_N - \partial_{\mu_j} H_N = v_j^2/2 + \mu_j^2/2 + \mu_j^{-1} v_j \partial_{v_j} V_N - \partial_{\mu_j} V_N. \end{aligned}$$

We remark that one can scale the Gross-Pitaevskii equation (1.6) in the following way: Consider any function $u(x, t)$, scaling parameter α , let $\tilde{x} = \alpha x$, $\tilde{t} = \alpha^2 t$, and define the new function

$$(3.9) \quad \tilde{u}(\tilde{x}, \tilde{t}) \stackrel{\text{def}}{=} \frac{1}{\alpha} u(x, t).$$

Then if $u(x, t)$ satisfies (1.6) with the potential $V(x)$, $\tilde{u}(\tilde{x}, \tilde{t})$ also satisfies (1.6) with the new potential

$$(3.10) \quad \tilde{V}(\tilde{x}) = \frac{1}{\alpha^2} V\left(\frac{\tilde{x}}{\alpha}\right).$$

This means that if we deal with a soliton of width comparable with α , the potentials for which interesting dynamics should appear should have size approximately α^{-2} and the slowly varying factor replaced by h/α .

The effective dynamics equations (3.8) scale similarly: if $(a(t), v(t), \theta(t), \mu(t))$ satisfies (3.8) and we define \tilde{x}, \tilde{t} , and \tilde{V} as above, then $(\tilde{a}(\tilde{t}), \tilde{v}(\tilde{t}), \tilde{\theta}(\tilde{t}), \tilde{\mu}(\tilde{t}))$ also satisfies (3.8) with

$$(3.11) \quad \tilde{a}(\tilde{t}) = \alpha a(t), \quad \tilde{v}(\tilde{t}) = \frac{v(t)}{\alpha}, \quad \tilde{\theta}(\tilde{t}) = \theta(t), \quad \tilde{\mu}(\tilde{t}) = \frac{\mu(t)}{\alpha}.$$

The scalings (3.9) and (3.11) are related in the following way: if

$$u(x, t) = q_N(x, a(t), v(t), \theta(t), \mu(t)),$$

then

$$\tilde{u}(\tilde{x}, \tilde{t}) = q_N(\tilde{x}, \tilde{a}(\tilde{t}), \tilde{v}(\tilde{t}), \tilde{\theta}(\tilde{t}), \tilde{\mu}(\tilde{t}))/\alpha = q_N(x, \tilde{a}(\tilde{t}), \tilde{v}(\tilde{t}), \tilde{\theta}(\tilde{t}), \tilde{\mu}(\tilde{t})).$$

4. COMPARISON OF EFFECTIVE AND EXACT DYNAMICS

For given values $a_0, v_0, \theta_0, \mu_0$ in \mathbb{R}^N , we consider the solution $u(\cdot, t)$ of (1.6) with initial data $q_N(\cdot, a_0, v_0, \theta_0, \mu_0)$ and the solutions $a(t), v(t), \theta(t), \mu(t)$ of the effective dynamics equations (3.8) with initial values $a_0, v_0, \theta_0, \mu_0$. In the following discussions we will refer to $u(\cdot, t)$ as the exact solution and $q_N(\cdot, a(t), v(t), \theta(t), \mu(t))$ as the effective dynamics.

Holmer and Zworski [8] proved that in the case $N = 1$,

$$(4.1) \quad \|u(\cdot, t) - q_N(\cdot, a(t), v(t), \theta(t), \mu(t))\|_{H^1} = Ch^{2-\delta}, \quad \text{for } t < \frac{\delta \log(1/h)}{Ch},$$

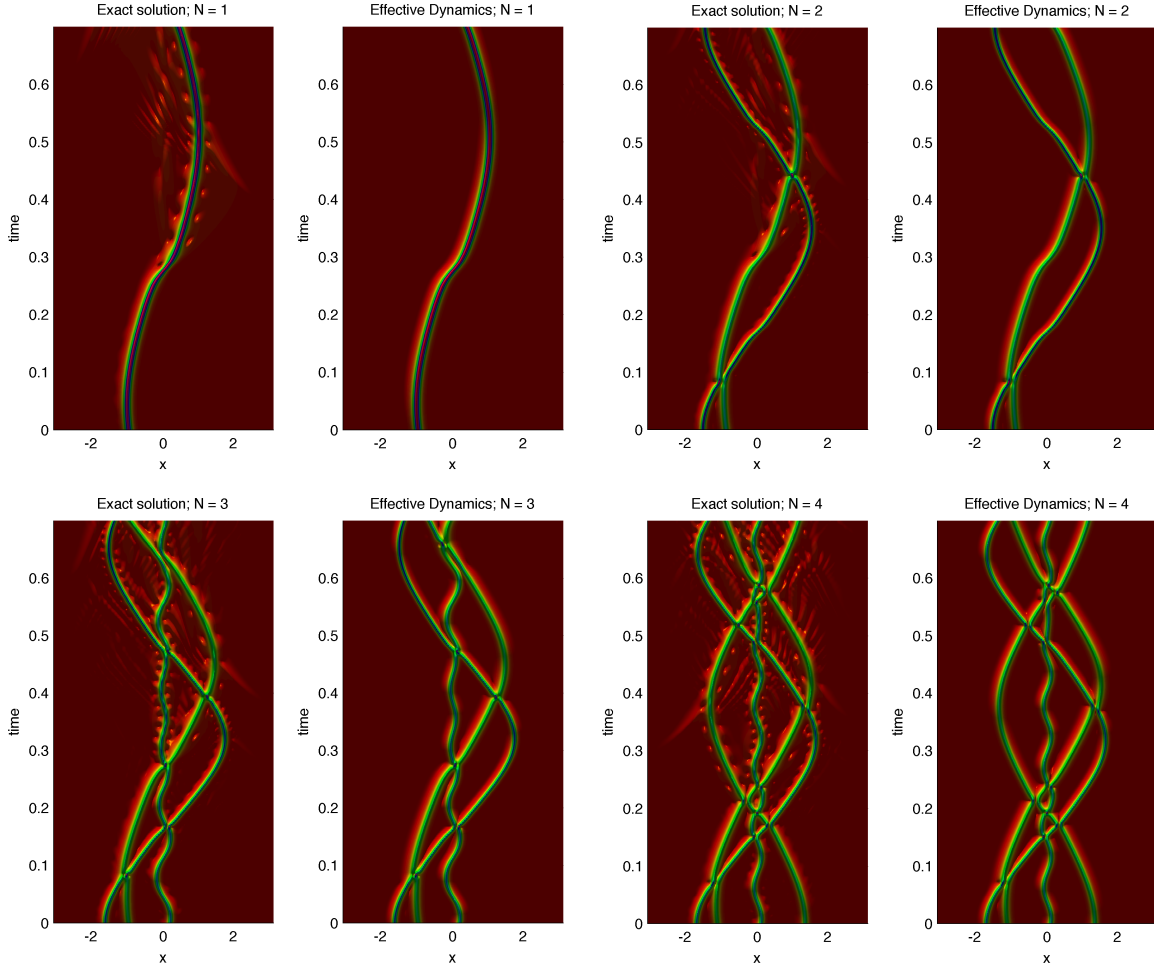


FIGURE 4. A side-by-side comparison of the absolute value of the exact solution of (1.6) versus the effective dynamics (3.8) for 1,2,3, and 4 solitons with potential $W(x) = -100 \operatorname{sech}^2(5x) + 10x^4$. The sharpness of the $\operatorname{sech}^2(5x)$ term creates clearly visible discrepancy between the two solutions.

where $\delta \in (0, 1/2)$ can be chosen, and where C depends only on the potential and initial velocity of the soliton, but not on δ . The H^1 norm measures the size of the function and its spatial derivative in L^2 :

$$\|v\|_{H^1}^2 \stackrel{\text{def}}{=} \|v\|_{L^2}^2 + \|\partial_x v\|_{L^2}^2, \quad \|v\|_{L^2}^2 \stackrel{\text{def}}{=} \int_{\mathbb{R}} |v(x)|^2 dx.$$

This norm measures the energy of the solution.

The limiting time $\log(1/h)/h$ is the Ehrenfest time discussed in §1.

It is expected that this result also holds for $N > 1$. This is suggested by [7], which proves the analogous theorem for the modified Korteweg-de Vries (mKdV) equations for case $N = 1, 2$, see §6 below. However, the methods of [7] do not fully apply to the case of the Gross-Pitaevsky equation (1.5). Also, even in the case of mKdV and $N = 2$, multiple

soliton interactions are not theoretically understood. All these considerations provided a strong motivation for this numerical study.

We note that for $N > 1$, it was conjectured in [7] that the error bounds (4.1) will hold not only in the H^1 norm, but for the H^N norm, which measures the size of a function and its first N derivatives, where N is the number of solitons. This has been proven in the mKdV case with $N = 2$ [7]. For our numerical experiments, we consider only the H^1 norm.

We present numerical simulations to show that the result (4.1) holds for $N > 1$ in the following three sections: In §4.1 we choose initial data and two potentials that demonstrate the power and limitations of the effective dynamics equations, regardless of the number of solitons. Using the same initial data and one of the potentials from §4.1, in §4.2 we verify that the $\mathcal{O}(h^{2-\delta})$ error estimate in (4.1) holds as $h \rightarrow 0$ for a fixed time interval. We then turn to the $\log(1/h)/h$ timescale, or Ehrenfest timescale, in §4.3 to show that it is the appropriate timescale for which we can expect (4.1) to hold.

4.1. A numerical case study. We consider initial data $q_N(\cdot, \bar{a}_N, \bar{v}_N, \bar{\theta}_N, \bar{\mu}_N)$, where $\bar{a}_N = (a_1, \dots, a_N)$, $N = 1, 2, 3, 4$ and $\bar{v}_N, \bar{\theta}_N$, and $\bar{\mu}_N$ are similarly defined with

$$(4.2) \quad \begin{aligned} (a_1, a_2, a_3, a_4) &= (-1, -1.5, 0, 1) \\ (v_1, v_2, v_3, v_4) &= (-2, 0, 3, 0) \\ (\theta_1, \theta_2, \theta_3, \theta_4) &= (\pi/3, 0, -3, -5) \\ (\mu_1, \mu_2, \mu_3, \mu_4) &= (17, 25, 23, 19) \end{aligned}$$

The positions and masses are chosen to satisfy a numerical requirement that $q_N(\cdot, \bar{a}_N, \bar{v}_N, \bar{\theta}_N, \bar{\mu}_N)$ is close to 0 outside of $(-\pi, \pi)$, our numerical domain (see §7). Rescaling the solution as in (3.9) or enlarging the numerical domain allows for data that does not satisfy this numerical requirement. The initial data is otherwise chosen arbitrarily.

We first consider the potential

$$V_1(x) = -100 e^{\cos x},$$

see Figure 3. The factor -100 is chosen to create a deep enough well so that the solutions remain in $(-\pi, \pi)$, but the potential is otherwise chosen arbitrarily.

We compute the exact solution and the effective dynamics solution for $N = 1, 2, 3, 4$ up to time $t = 1$, which is chosen to allow for multiple soliton interactions. We plot the solution for 4 solitons in Figure 1, where we observe very little difference between the exact and effective dynamics solutions. An equally small amount of discrepancy between the solutions was observed for $N = 1, 2, 3$.

Next, we consider the same initial data as above with the potential

$$V_2(x) = -100 \operatorname{sech}^2(5x) + 10x^4,$$

see Figure 3. This potential is chosen to be outside of the slowly varying regime for which the effective dynamics give good approximations. This is due to the $-100\operatorname{sech}^2(5x)$ term, which creates a sharp dip roughly the width of the solitons we are studying; thus we do not expect the exact solution to maintain its soliton structure very well. This causes the

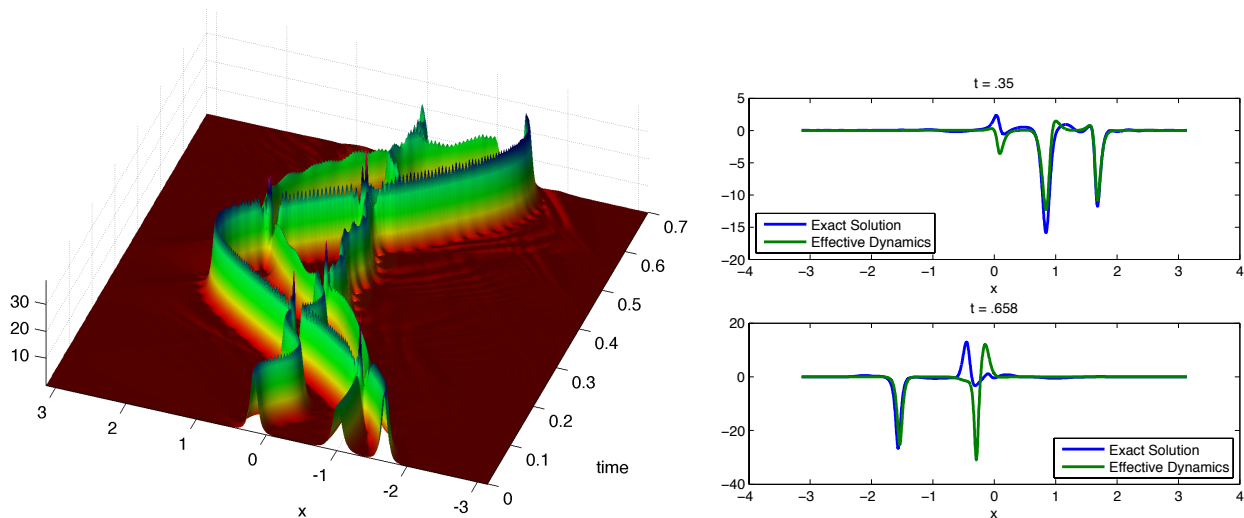


FIGURE 5. The plot on the left is a different view of the exact solution with 3 solitons shown in Figure 4. The plot on the right compares the real parts of the $N = 3$ exact solution with the effective dynamics solution at times $t = 0.35$ and $t = 0.658$.

clearly visible discrepancies between the effective dynamics and the exact solution in Figure 4. The $10x^4$ term ensures the solutions remain on the interval $(-\pi, \pi)$.

We compute the solutions for $N = 1, 2, 3, 4$ up to time $t = 0.7$, which is again chosen to allow for multiple soliton interactions. Figure 4 displays these solutions and demonstrates that the effective dynamics captures the true motion, regardless of the number of solitons and regardless of multiple soliton interactions. In the experiments presented in this paper, we only consider $N \leq 4$, but we have observed good agreement between the exact solution and the effective dynamics for $N \leq 7$. We did not investigate further due to increasing computational time needed to solve (3.8).

We note that for $N \geq 2$ the phases of the solitons are crucial in determining the interaction between solitons. In Figure 4, we see that for $N = 3$, at approximately $t \approx 0.65$, two solitons that appear to bounce off each other in the exact solution instead appear to cross in the effective dynamics. This discrepancy seems to be due to differences between exact phases and effective phases. In Figure 5 we are able to see large deviation in the phases between the exact solution and effective dynamics by comparing the real part of the solutions.

4.2. Quantitative study of the error as $h \rightarrow 0$. We investigate the $\mathcal{O}(h^{2-\delta})$ error between the exact solution and the effective dynamics on a fixed time interval. The estimate that gives rise to (4.1) is

$$(4.3) \quad \|u(\cdot, t) - q_N(\cdot, a(t), v(t), \theta(t), \mu(t))\|_{H^1} \leq Ch^2 e^{Cht}.$$

If $t = \delta \log(1/h)/(Ch)$, then the RHS reduces to $Ch^{2-\delta}$. When dealing with fixed length of time or even time of size $\mathcal{O}(1/h)$ the RHS is $\mathcal{O}(h^2)$ and that form of error will be shown to be optimal.

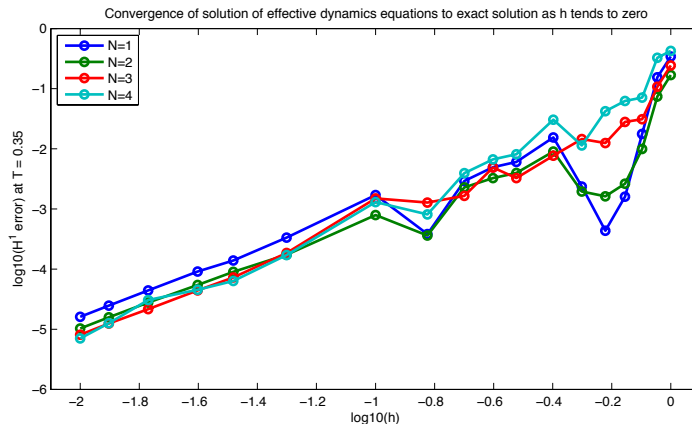


FIGURE 6. A log-log plot of the H^1 error, relative to the H^1 norm of the initial data, between the exact solution of 1.6 and the N -soliton evolving according to the effective dynamics equations 3.8, as function of h . Here, the potential is $V(x) = W(hx)$, where $W(x) = -100 \operatorname{sech}^2(5x) + 10x^4$. For smaller values of h , the slope of the lines approaches 2, in agreement with the theoretical upper bound on the error in (1.8).

We reconsider our second potential from §4.1, but add the slowly varying parameter, h :

$$V(x) = W(hx), \quad W(x) = -100 \operatorname{sech}^2(5x) + 10x^4,$$

and explore the H^1 error, relative to the H^1 norm of the initial data, between the exact solution and effective dynamics as $h \rightarrow 0$. We expect that as h becomes small enough, the equation will enter the slowly varying regime and display $\mathcal{O}(h^2)$ error. Indeed, the log-log plot in Figure 6 demonstrates the error is bounded by $C_N h^2$ as $h \rightarrow 0$, where the constant C_N varies only slightly between different values of N .

We fit the data from Figure 6 to a line using the 6 smallest values of h .

N	1	2	3	4
Slope	1.86	1.76	1.91	1.86
C_N	-1.07	-1.46	-1.27	-1.37

Thus, we conclude that the error is approximately $\mathcal{O}(h^2)$.

4.3. Ehrenfest time. We now investigate the length of time for which the effective dynamics approximation is accurate. In (4.3), we recalled that the error is bounded by $Ch^2 e^{Cht}$ and hence the approximation breaks down at the Ehrenfest time,

$$T(h) \sim \log(1/h)/h.$$

We have already verified for small h and fixed time this error behaves as $\mathcal{O}(h^2)$. Thus we focus on observing exponential growth in the error as a function of time, and verifying that it is of the form $\mathcal{O}(e^{Cht})$.

For this we must choose a potential and initial data to exhibit exponential instability. We are motivated by Newton's equations for $V(a) = -a^2/2$:

$$(4.4) \quad \dot{a} = v, \quad \dot{v} = a, \quad v = v_0 \cosh t + a_0 \sinh t, \quad a = a_0 \cosh t + v_0 \sinh t.$$

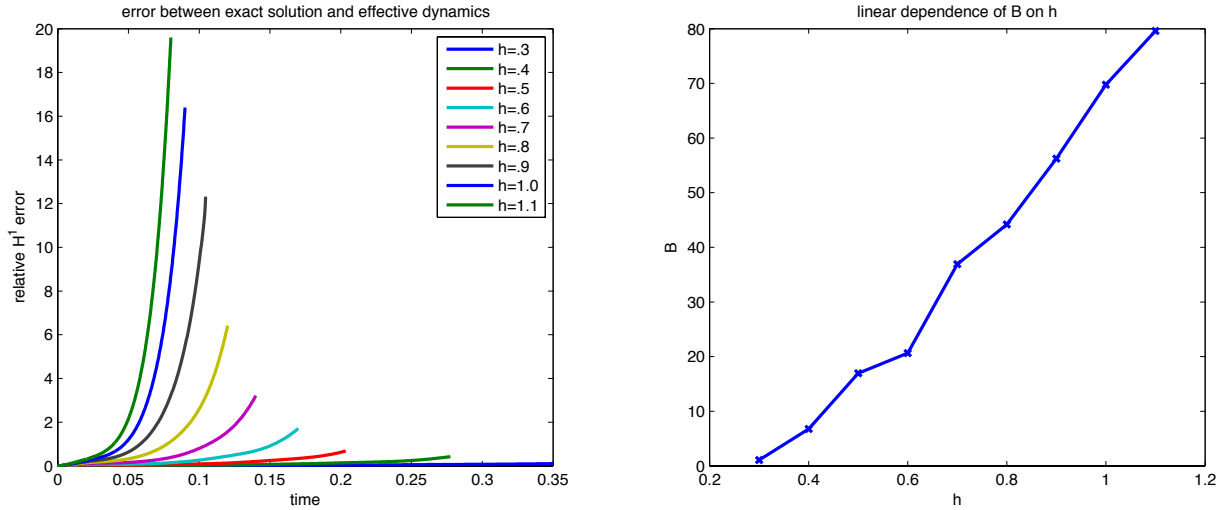


FIGURE 7. The plot on the left shows H^1 error, relative to the H^1 norm of the initial data, between the exact solution of (1.6) and the effective dynamics for a single soliton sliding down the concave potential $V(x) = W(hx)$, where $W(x) = 1000x^2$. The error is plotted as a function of time and for several values of the parameter h . On the right side, B is plotted as a function of the parameter h , when the errors from the plot on the left are fitted to a curve of the form $A(e^{Bt} + C)$. We expect B to depend linearly on h .

In this case, we have exponential instability of classical dynamics. This suggests choosing potentials with a non-degenerate maximum and working near the unstable equilibrium points.

Hence we will investigate solutions to (1.6) with potential

$$V(x) = W(hx), \text{ where } W(x) = -1000x^2.$$

Figure 7 below demonstrates exponential divergence between the exact solution to (1.6) and the effective dynamics for several values of h and a single soliton initial condition $q_1(x, .1, 0, 0, 15)$.

We fit the plots shown in Figure 7 to a function of the form $A(e^{Bt} + C)$, for the time period when the soliton's position was between $x = .15/h$ and $x = 1.2/h$. This range was observed to be a region where exponential increase dominated the error and before the soliton approached the numerical boundary.

In Figure 7 we observe a linear dependence of B on h , in agreement with (4.3). This indicates that for certain potentials the Ehrenfest time $C \log(1/h)/h$ is the appropriate bound for the length time we expect the effective dynamics to give a good approximation to (1.6). We note that in our experiments with other potentials we often observe a linear increase in error which would correspond to a timescale of C/h^2 instead of the Ehrenfest time $C \log(1/h)/h$.

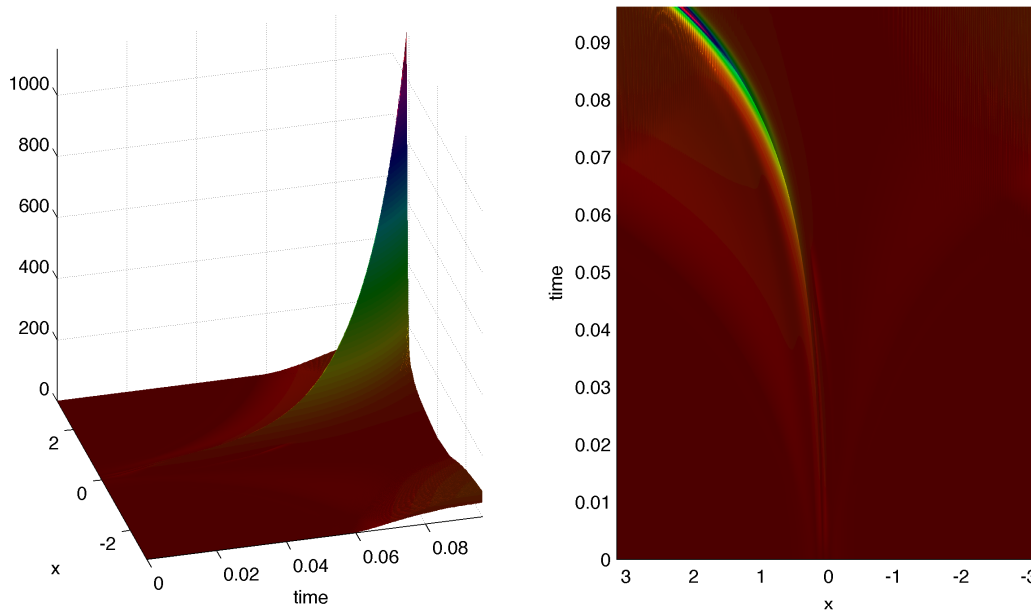


FIGURE 8. Surface plots of the error between the exact solution of (1.6) and the effective dynamics for a single soliton sliding down the concave portion of the potential $V(x) = W(hx)$, where $W(x) = 1000x^2$, as in Figure 7. We have plotted the absolute value of the difference between the spatial derivatives between the two solutions.

5. APPLICATION TO BOSE-EINSTEIN CONDENSATES

Strecker, Partridge, Truscott and Hulet [14] discovered that Bose-Einstein condensates form stable soliton trains while confined to one-dimensional motion. When set into motion in a suitably chosen optical trap, a Bose-Einstein condensate forms multiple soliton formations which exist for multiple oscillatory cycles without being destroyed by dispersion or diffraction. We can observe this same behavior numerically, using the effective dynamics equations. We choose a potential of the type described in [14]

$$V(x) = \left(\frac{x}{2}\right)^6$$

and set $N = 4$, which was the most frequent case in their experiment. Strecker *et al* inferred that the repulsive behavior of the solitons indicated alternating phases. Their argument was based on considering a certain reduced Lagrangian.

In our numerical experiment we put $\bar{\theta} = (0, \pi, 0, \pi)$ and then set the four solitons in motion with the same velocity near the center of the potential. Similar to [14], we observe bunching and spreading of the soliton train for several oscillations. See Figure 2.

6. EFFECTIVE DYNAMICS FOR THE mKdV EQUATION

The mKdV equation

$$(6.1) \quad \partial_t u = -\partial_x(\partial_x^2 u + 2u^3),$$

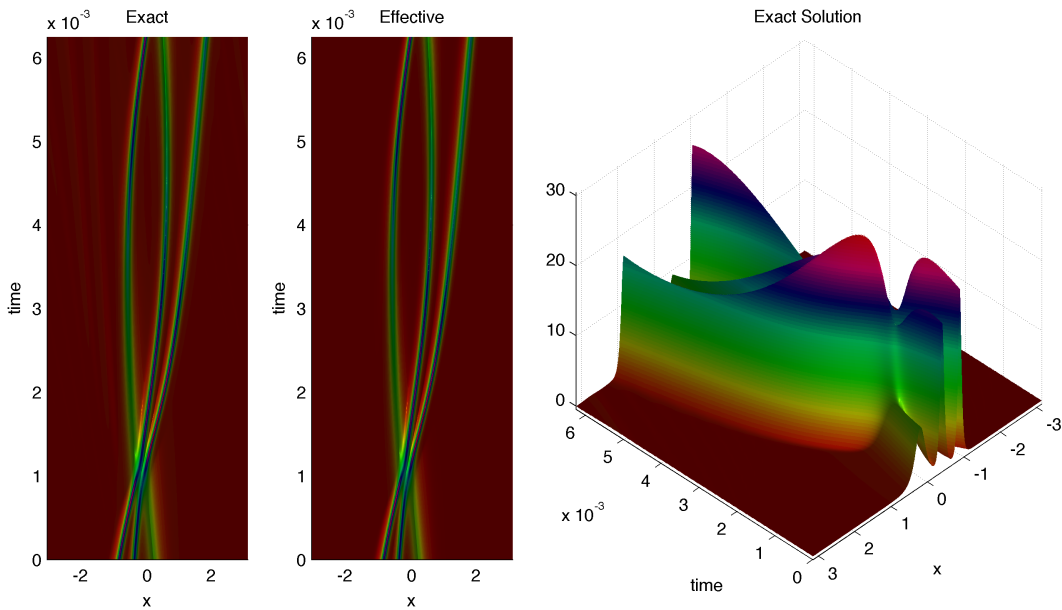


FIGURE 9. The left plot shows a side-by-side comparison of the exact solution of the mKdV equation (6.2) and the effective dynamics solution for 3 solitons with potential $b(x) = 300 \cos^2 x$. No discrepancy between the two solutions is visible. The right plot displays the exact solution from a different angle.

like the nonlinear Schrödinger equation, has soliton solutions and a Hamiltonian structure. Holmer, Perelman, and Zworski [7] derived effective dynamics equations for the mKdV equation with a slowly varying potential

$$(6.2) \quad \partial_t u = -\partial_x(\partial_x^2 u - b(x, t)u + 2u^3), \quad b(x, t) = b_0(hx, ht)$$

and proved a result analogous to the (4.1) for $N = 1, 2$: the H^N error between the solution of (6.2) and its associated effective dynamics with N -soliton initial data is bounded by

$$(6.3) \quad Ch^2 e^{Cht}, \quad \text{for } t < \frac{C}{h} \log \frac{1}{h},$$

Similarly to §4.2, we have conducted a numerical study verifying that the H^1 error is $\mathcal{O}(h^2)$ as $h \rightarrow 0$ for multiple soliton initial conditions. See Figures 9 and 10.

7. NUMERICAL METHODS

We now describe the numerical methods we employ to compute the Gross-Pitaevskii PDE (1.6) and the ODE (3.8) arising from the effective dynamics. When comparing a solution of (1.6) with a solution of (3.8), we refine our numerical solutions until the error between successive refinements of solutions to the same equation is several orders of magnitude smaller than the error between solutions of the two equations.

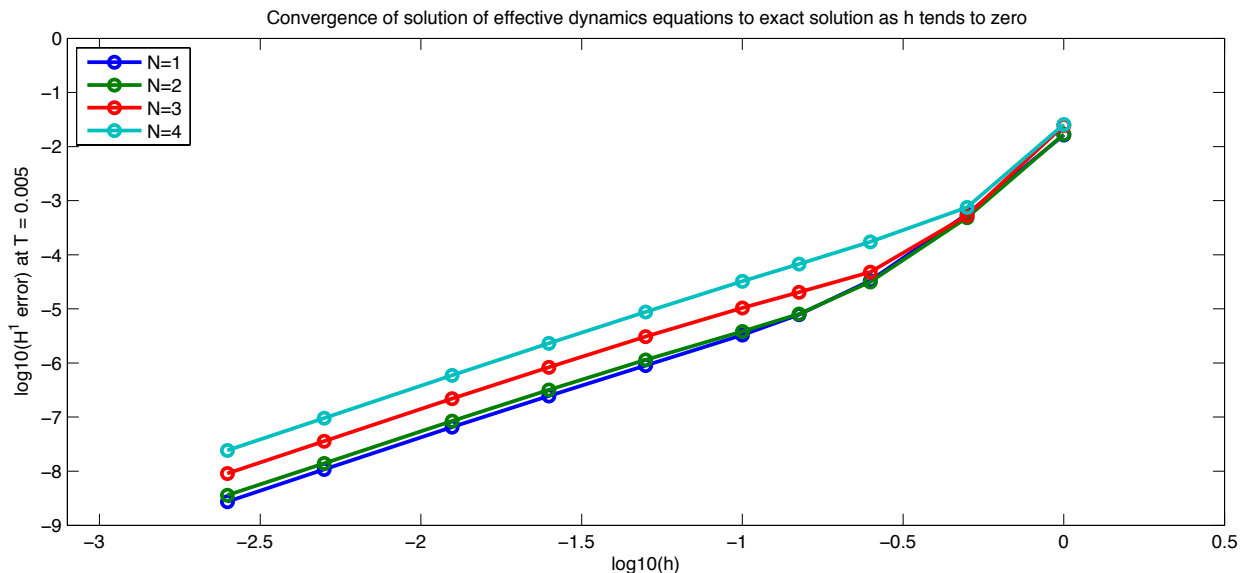


FIGURE 10. A log-log plot of the H^1 error, relative to the H^1 norm of the initial data, between the exact solution to the mKdV equation (6.2) and the N -soliton evolving according to the effective dynamics, as a function of h . For smaller values of h , the slope of the lines approaches 2, in agreement with the theoretical upper bound on the error. The theoretical upper bound has only been proven for $N = 1, 2$, but this figure gives evidence that it holds for all N .

Numerically solving the ODE arising from the effective dynamics (3.8) necessitates computing $q_N(x, a, v, \theta, \mu)$ and its derivatives with respect to the parameters a, v, θ , and μ efficiently. For this we note that an equivalent definition of q_N in (2.5)

$$(7.1) \quad q_N(x) = -\vec{1}M^{-1}\gamma,$$

where $\vec{1}$, M , and γ are as in (2.5). Since iM is Hermitian, $M^{-1}\gamma$ can be efficiently computed using the Cholesky factorization. Differentiating q_N numerically, for larger values of N , is too costly. Instead we used (7.1) to obtain explicit formulas for the derivatives of q_N and again used Cholesky factorizations to efficiently compute them. With this we compute the integrand in (3.6), and then numerically integrate it using the trapezoidal method. Once we can efficiently compute the RHS of the effective dynamics equations (3.8), the standard fourth-order Runge Kutta method was found to be suitable to solve to the ODE.

In order to solve the PDE (1.6) we used a Fourier spectral method to study the evolution on the numerical domain $(-\pi, \pi)$. This requires our solution $u(x, t)$ to be periodic in space, so we choose initial conditions such that $u(x, t)$ decays to zero, to machine precision, before the endpoints $-\pi$ and π . Arbitrary initial data can be handled by either extending the numerical domain or rescaling the equation (see (3.9)).

One difficulty arises in that a non-trivial potential $W(hx)$ cannot be periodic for all h . However, the potential $W(hx)$ need not be periodic on $(-\pi, \pi)$ so long as the product $W(hx)u(x, t)$ is periodic on $(-\pi, \pi)$, which is achieved if $u(x, t)$ decays fast enough at the endpoints $-\pi$ and π . If $W(x)$ is periodic on $(-\pi, \pi)$ and one wishes to consider a

solution $u(x, t)$ that doesn't decay before the endpoints $-\pi$ and π , the rescaling (3.9) may be employed with $\alpha = h$:

$$(7.2) \quad \tilde{x} = hx, \quad \tilde{t} = h^2t, \quad \tilde{u}(\tilde{x}, \tilde{t}) \stackrel{\text{def}}{=} \frac{1}{h}u(x, t).$$

Then if $\tilde{u}(\tilde{x}, \tilde{t})$ satisfies (1.6) with periodic potential $\tilde{V}(\tilde{x}) = W(\tilde{x})/h^2$, $u(x, t)$ also satisfies (1.6) with potential $V(x) = W(hx)$.

This rescaling also makes it clear that as $h \rightarrow 0$, a soliton solution becomes sharper relative to the potential. This requires higher resolution in order to apply our numerical method to solve the PDE (1.6), while the effective dynamics equations (3.8) are unaffected. Indeed, our numerical experiments confirmed that increased computational effort was needed to resolve the PDE as $h \rightarrow 0$, but not the effective dynamics ODE.

We now describe the method to solve a general solution $u(x, t)$ of (1.6) on a periodic domain with periodic initial data and potential $V(x)$. The Fourier modes $\hat{u}_k(t)$ of a solution $u(x, t)$ to (1.6) evolve according to

$$(7.3) \quad \partial_t \hat{u}_k = -\frac{i}{2}k^2 \hat{u}_k + i(\widehat{uv})_k, \quad v = |u|^2 - V$$

Discretizing space and replacing the Fourier Transform with the Discrete Fourier Transform gives rise to a finite dimensional system of ODE, which we now represent in the general form

$$(7.4) \quad u_t = \mathcal{L}u + \mathcal{N}(u)$$

where \mathcal{L} is a stiff linear transformation corresponding to the first term of (7.3) (represented by a diagonal matrix in our case) and \mathcal{N} is a non-linear operator from the second term of (7.3). To solve (7.4) we compared the fourth order implicit-explicit (IMEX) method ARK4(3)6L[2]SA proposed by Kennedy and Carpenter [10] with the exponential time differencing (ETD) method ETD4 proposed by Kassam and Trefethen [9]. The IMEX scheme update formula is

$$(7.5) \quad u_{n+1} = u_n + \Delta t(b_1(k_1 + l_1) + \cdots + b_s(k_s + l_s)),$$

where Δt is the time step and k_i and l_i are chosen such that

$$(7.6) \quad k_i = \mathcal{L}(u_n + \Delta t(A_{i1}k_1 + \cdots + A_{is}k_s + \hat{A}_{i1}l_1 + \cdots + \hat{A}_{is}l_s))$$

$$(7.7) \quad l_i = \mathcal{N}(u_n + \Delta t(A_{i1}k_1 + \cdots + A_{is}k_s + \hat{A}_{i1}l_1 + \cdots + \hat{A}_{is}l_s)).$$

Here A, \hat{A} are $s \times s$ lower triangular matrices with \hat{A} having zeros along its diagonal. This allows us to solve for the k_i and l_i one stage at a time, only inverting the diagonal linear operators $I - \Delta t A_{ii} \mathcal{L}$. The implicit treatment of the \mathcal{L} term mitigates the stiffness arising from the k^2 factor in (7.3), while the l_i can be computed explicitly, so non-linear equations involving \mathcal{N} need not be solved.

The ETD method, on the other hand, uses an exact formula for obtaining the next step u_{n+1} from u_n based on solving the linear portion exactly:

$$(7.8) \quad u_{n+1} = e^{\mathcal{L}\Delta t}u_n + e^{\mathcal{L}\Delta t} \int_0^{\Delta t} e^{-\mathcal{L}\tau} \mathcal{N}(u(t_n + \tau), t_n + \tau) d\tau$$

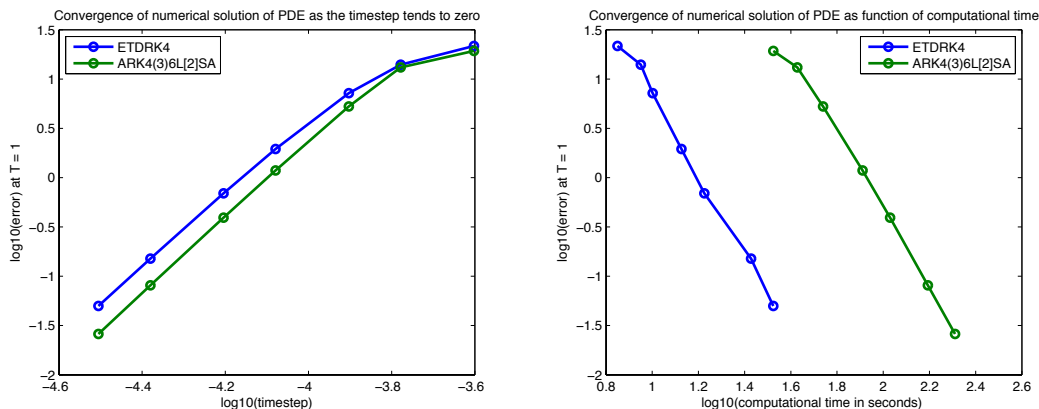


FIGURE 11. Log-log plots of the convergence of the fourth order schemes ETDRK4 and ARK4(3)6L[2]SA as a function of the timesteps and computational time, respectively. ARK4(3)6L[2]SA is slightly more efficient per timestep, but ETDRK4 is significantly more computationally efficient.

The integral in (7.8) can then be numerically approximated using matrix exponents of \mathcal{L} and evaluations of N . Thus as with the IMEX method, we do not need to solve non-linear equations, and computations involving \mathcal{L} (namely computing $e^{\Delta t \mathcal{L}}$) are efficient because \mathcal{L} is diagonal. Stiffness is mitigated by solving the linear portion of (7.4) exactly. We found that the ETDRK4 scheme computed a solution of a desired accuracy nearly twice as fast as the ARK4(3)6L[2]SA scheme. While the ARK4(3)6L[2]SA scheme had a slightly smaller error rate per step, more computations per step made it significantly less efficient. Neither method demonstrated any instability in the range of step sizes required for our solutions. Below, we plot the convergence of the two schemes as the timestep goes to zero. To obtain the results in the figures, we used the same potential and initial data as in §4.1: $W(x) = -100 \operatorname{sech}^2(5x) + 10x^4$.

Acknowledgements. The author was supported through the National Science Foundation through grant DMS-0955078 and by the Director, Office of Science, Computational and Technology Research, US Department of Energy under Contract DE-AC02-05CH11231. The author would like to thank Jon Wilkening and Maciej Zworski for helpful discussions and comments.

REFERENCES

1. S. De Bièvre and D. Robert, *Semiclassical propagation on $|\log \hbar|$ time scales*, Int. Math. Res. Not. **12** (2003), 667–696.
2. R. Carles, *Semi-classical analysis for nonlinear schrödinger equations*, World Scientific Publishing Co. Pte. Ltd., Hackensack, NJ, 2008.
3. L.D. Faddeev and L.A. Takhtajan, *Hamiltonian methods in the theory of solitons*, Springer, Berlin, 1987.
4. J. Fröhlich, S. Gustafson, B.L.G. Jonsson, and I.M. Sigal, *Solitary wave dynamics in an external potential*, Comm. Math. Physics **250** (2004), 613–642.
5. R.H. Goodman, P.J. Holmes, and M.I. Weinstein, *Strong nls soliton-defect interactions*, Physica D **192** (2004), 215–248.
6. G. Hagedorn, *Semiclassical quantum mechanics*, Ann. Phys. **135** (1981), 5870.

7. J. Holmer, G. Perelman, and M. Zworski, *Soliton interaction with slowly varying potentials*, preprint. [arXiv:0912.5122](https://arxiv.org/abs/0912.5122) (2008).
8. J. Holmer and M. Zworski, *Soliton interaction with slowly varying potentials*, IMRN **2008** (2008), Art. ID runn026, 36 pp.
9. A. Kassam and L. N. Trefethen, *Fourth-order time-stepping for stiff pdes*, Siam J. Sci. Comput. **26** (2005), 1214–1233.
10. C. A. Kennedy and M. H. Carpenter, *Additive runge-kutta schemes for convection-diffusion-reaction equations*, Applied Numerical Mathematics **44** (2003), 139–181.
11. Y.S. Kivshar and B.A. Malomed, *Dynamics of solitons in nearly integrable systems*, Rev. Mod. Phys. **61** (1989), 763–915.
12. L.P. Pitaevskii and S. Stringari, *Bose-Einstein condensation*, Oxford: Clarendon Press, 2003.
13. D. Robert, *On the herman-kluk semiclassical approximation*, arXiv 0908.0847, 2009.
14. K.E. Strecker, G.B. Partridge, A.G. Truscott, and R.G. Hulet, *Formation and propagation of matter-wave soliton trains*, Nature **417** (2002), 150–153.

DEPARTMENT OF MATHEMATICS, UNIVERSITY OF CALIFORNIA, BERKELEY, CA 94720, USA

E-mail address: potter@math.berkeley.edu